Vol. 92: 1–20, 2024
https://doi.org/10.3354/cr01730

CLIMATE RESEARCH
Clim Res

Published January 18

Contribution to CR Special 36 'Observed changes in climate over Asia'

Temporal characteristics of extreme high temperatures in Wuhan since 1881

Xiang Zheng[1], Guoyu Ren[1,2], Jiajun He[1,*], Yuxinzi Zhao[1,3], Yuyu Ren[2], Guowei Yang[4]

[1]Department of Atmospheric Science, School of Environmental Studies, China University of Geosciences (CUG), Wuhan 430074, PR China

[2]Laboratory for Climate Studies, National Climate Center, China Meteorological Administration (CMA), Beijing 100081, PR China

[3]Jiangling Meteorological Service, Jiangling 434100, PR China

[4]Division of Climate Change Monitoring and Projection, National Climate Centre, China Administrational Administration (CMA), Beijing 100081, PR China

ABSTRACT: The construction and analysis of daily temperature data series in long enough a time period is important to understand decadal to multi-decadal variability and changing trends in extreme temperature events. This paper reports a new analysis of extreme temperature indices over the last 140 yr in Wuhan, China, with an emphasis on changes in extreme high temperature changes. The daily temperature data from 9 stations from 1881 to 1950 and 1 modern station from 1951 to 2020 were used for the analysis. Based on the data, and the commonly used extreme temperature indices, the variations and long-term trends of extreme high temperature events in Wuhan since 1881 were analyzed. The results show that there was no clear warming trend in maximum temperature, but a quite large inter-annual and inter-decadal fluctuation. In contrast, there was a very significant increase in minimum temperature, with a large upward trend overall. The extreme temperature indices exhibit a periodic variability, and frequent extreme heat events have been experienced over the last 140 yr in Wuhan. Most extreme temperature indices did not exhibit remarkable changes during the first half of the period analyzed. However, the majority of the extreme temperature indices showed significant upward trends over the latter half of the 140 yr period. The possible causes of the observed changes in the extreme high temperature events in the different time periods are also discussed.

KEY WORDS: Daily data · Extreme high temperature · Centennial scale · Variation characteristics · Average temperature · Wuhan City

1. INTRODUCTION

Climate change has a significant impact on natural and human systems (Handmer et al. 2012, Sun et al. 2016, Luo & Lau 2021, Zhang et al. 2023). Instrumental data have clear advantages in the study of the characteristics and mechanism of climate change. Detection and attribution of climate change signals often rely on long-term recorded instrumental data (Rasmussen et al. 2012). Moreover, instrumental data are more representative and accurate than other meteorological data (such as reanalysis data and modeling data) (Lee et al. 2011). However, due to many factors, there are problems with instrumental data for earlier periods (Shen & Somerville 2019), such as the sparsity of observation stations, and missing data from war or accidental fires. In addition, migration of sites and instrumentation will lead to inhomogeneity of the observation data in sub-periods of the early-year observations (Yang et al. 2013).

*Corresponding author: jiajun.he@cug.edu.cn

Publisher: Inter-Research · www.int-res.com

Based on meteorological station records from various continents across the globe, several representative long-term observational temperature datasets ranging over 100 yr have been developed (e.g. Jones et al. 2012, Rohde et al. 2013, Menne et al. 2018, Lenssen et al. 2019). However, these datasets were established on monthly scales. In the analysis of extreme climate change, daily surface air temperature (SAT) data are more useful than monthly temperature data and can provide more detailed information (Vincent et al. 2012, Hewaarachchi et al. 2017). Due to the lack of observation data for early periods, previous analysis of extreme climate change has focused mainly on the past 50 or 60 yr. In certain regional areas, such as some cities in Italy, France, Norway, Britain, Australia, and Japan (Camuffo 2002, Yan et al. 2002, Ansell et al. 2006, Zaiki et al. 2006, Cornes 2008, Ashcroft et al. 2014, Hestmark & Nordli 2016), the availability of daily instrumental observations extends back to earlier periods (before the 1950s), and even to the late 19th century, making them particularly valuable.

In China, some studies of extreme temperature index changes based on relatively long series have been carried out in some cities. For example, studies in Hong Kong have shown that extreme daily minimum and maximum temperatures, and the length of warm periods exhibit a long-term upward trend (1885–2008) (Lee et al. 2011). In Yingkou, Northeast China, the maximum, minimum, and average temperatures showed an increasing trend during 1904–2017, with the most significant increase occurring in daily minimum temperature (Xue et al. 2021). In Changchun, the number of warm days, high temperature days, and extreme maximum temperature values decreased during 1909–2018, while the extreme high temperature indices did not change significantly (Yu et al. 2020). Since these daily series start from an earlier observation period, they are particularly useful in the analysis of mesoscale and sub-seasonal extreme climate variations.

Wuhan, which has been named as one of the 'Four Stoves' in China, often suffers from extreme high temperature weather (Rong 2010). The temperature variability severely affects summer mortality in Wuhan. When the summer extreme high temperature sharply increases, the mortality rate also significantly rises in the city (Xu et al. 2016, Zhang et al. 2017). Extreme high temperature in Wuhan also negatively affects the supply of energy and water resources, especially in combination with extreme low mid-summer rainfall. Therefore, the study of extreme heat events in Wuhan is of great scientific significance and social value. The construction of high-resolution temperature observation data on a century scale is thus urgently needed. This will contribute to the study and analysis of the characteristics and trends of extreme weather changes in different periods in this region.

In addition, Chinese researchers have also conducted numerous studies on establishing long-term temperature and precipitation time series in China, often relying on proxy data such as tree rings, ice cores, and historical records to restore climate series before 1950 (Zheng et al. 2015, Yu et al. 2018, Wang et al. 2000). Although these results carry significant importance, revealing cyclical patterns and multi-scale climate variabilities over the past century, they are inadequate for quantitative monitoring and detection of long-term extreme climate events.

Although Wuhan has 100 yr of meteorological observation history, with the earliest observations beginning in 1869, the early meteorological data still requires further exploration and reconstruction. It is necessary to interpolate the missing data and perform a series of subsequent processing to obtain a sufficiently long temperature series that can be used for long-term extreme climate analysis. In addition, the analysis of extreme temperature change on a century scale for the city is still deficient. For a deeper and more comprehensive understanding of the long-term changes in mean and extreme climates in Wuhan, it is essential to conduct a detailed and thorough study of these extreme high temperature event changes.

In this study, the long-term daily temperature data series for Wuhan since 1881 was reconstructed, and the long-term change characteristics of the extreme high temperature indices were systematically analyzed. The results show a few interesting observed changes in extreme high temperature events, which will help deepen our understanding of long-term climate changes in this large city in Central China.

2. DATA AND METHODS

2.1. Data collection and stations information

The sub-daily meteorological records prior to 1951 were collected from the Atmospheric Circulation Reconstruction over the Earth (ACRE) project (Allan et al. 2011) and the National Meteorological Information Center (NMIC), China Meteorological Administration (CMA), and the modern daily meteorological records from 1951 to 2020 (WMO Station ID: 57494) were provided by the NMIC. The early sub-daily temperature

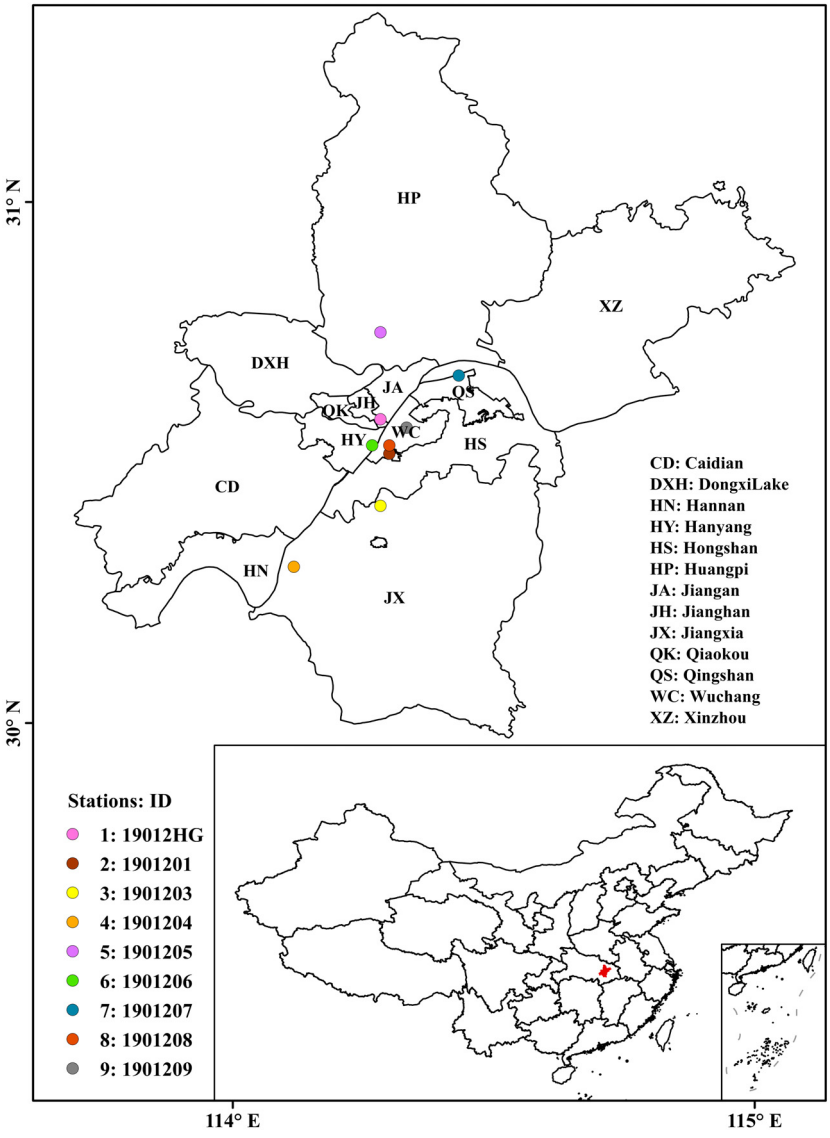

Fig. 1. Geographical distribution of the 9 early stations in Wuhan. The location of Wuhan is shown in red on the map of China

records for 1881–1950 came from 9 early stations in the Wuhan region (Fig. 1). Details of these 9 stations are shown in Table 1 & Fig. 2. The early data collected from these stations were quality controlled and homogenized in this study, which had not been conducted previously. The metadata (i.e. documents that record historical information such as station movements, thermometer replacements, environmental changes, etc.) from the national surface meteorological stations (including the modern Wuhan station) were accessed from the Meteorological Data Office of the NMIC. Wuhan station is one of the World Meteorological Organization (WMO) Centennial Observing Stations. The 20th century changes in SAT in Wuhan have been analyzed by Qin et al. (2000), Zheng et al. (2002), and Ren et al. (2010), based on monthly mean SAT data since 1905. Daily SAT data with observations over 100 yr was not previously available. Therefore, the daily dataset used in this study was developed by our group with the support of the Chinese National Key R&D project.

The data processing included the following steps: (1) digitizing instrumental data; (2) quality control; (3) metadata checking; (4) temporal interpolation of missing data; (5) data merging; and (6) data homogenization.

Quality control was carried out using the RClimdex software (Zhang & Yang

Table 1. Details of the 9 early stations and the modern station. Due to numerous minor gaps in the early observation data, only the earliest start and latest end times of each series are given. The detailed data distribution is shown in Fig. 2. Dates are given as yr/mo/d

Station ID	Lat. (°N)	Long. (°E)	Altitude (m)	Data source	Data period
19012HG	30.58	114.28	33.1	Other meteorological observations	1905/02/01–1941/05/31
1901201	30.52	114.30	18.8	Meteorological observation at university stations	1929/12/01–1949/12/31
1901203	30.42	114.28	49.0	Meteorological observation at university stations	1937/01/01–1955/06/30
1901204	30.30	114.12	23.2	Airport observation	1948/10/01–1951/12/31
1901205	30.75	117.28	29.1	Meteorological observation at hydrological stations	1950/01/01–1952/12/31
1901206	30.53	114.27	23.2	Airport observation	1952/07/01–1953/12/31
1901207	30.67	114.43	40.0	Other meteorological observations	1915/10/03–1918/12/31
1901208	30.53	114.30	33.5	Meteorological observation at university stations	1936/1/1–1937/09/30
1901209	30.57	114.33	48.0	Meteorological observation at customs stations	1880/03/01–1928/12/31
57494	30.60	114.05	23.6	Modern meteorological observation	1951/01/01–2020/12/31

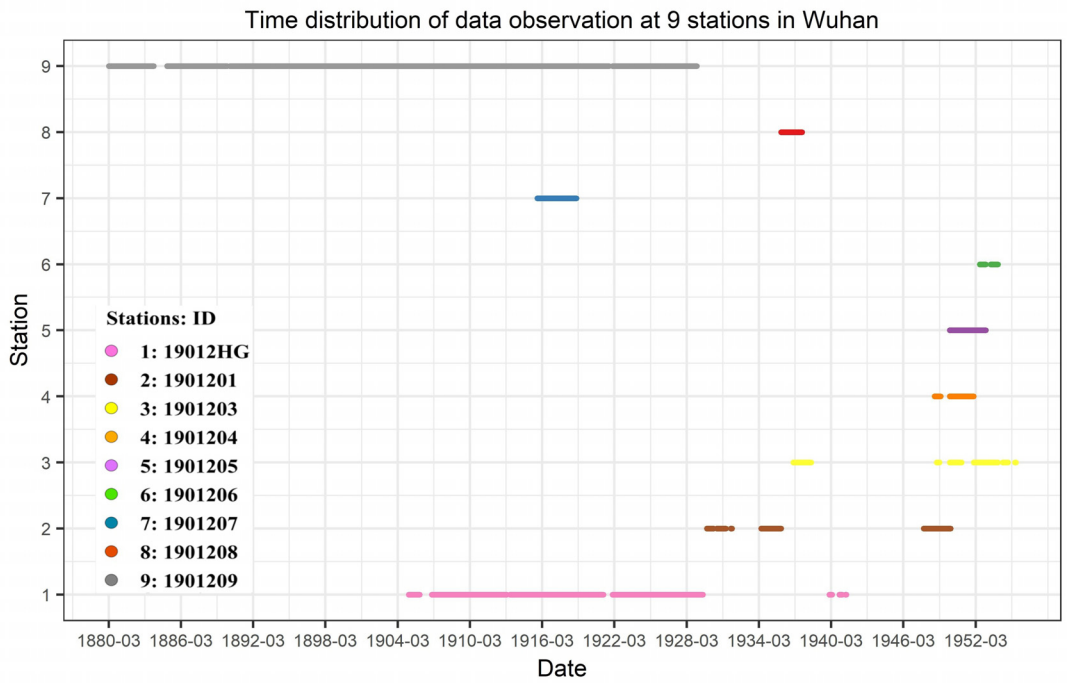

Fig. 2. Time distributions of observational records at the 9 early stations in Wuhan

2004). The main steps included a space consistency check, time consistency check, threshold value check, and extreme value check. Manual verification and correction were implemented in the time consistency check. The ridge regression model was used as the temporal interpolation method to reconstruct the missing data of maximum temperature (T_{max}) and minimum temperature (T_{min}). The main idea and steps of the interpolation method are explained in detail in Section 2.2. The RHtestv4 software (Wang & Feng 2013) was used to test and adjust the inhomogeneities of the daily temperature data. Detailed steps of the homogenization are provided in Section 2.3.

After data processing, the 140 yr daily T_{max} and T_{min} time series of Wuhan were established. The daily temperature series are shown in Fig. 4; there was a lack of measurements during 1940–1950, mainly due to the influence of the wars.

2.2. Interpolation and statistical methods

2.2.1. Ridge regression

In this study, ridge regression (Hoerl & Kennard 1970) was used as the temporal interpolation method. This method is employed to solve the problem of failure of least squares estimation under multicollinearity. It can be used to screen variables when too many variables are introduced and there are multiple collinearities, which make it difficult to decide which variable to leave. Ridge regression is a supplement to least squares regression.

Ordinary least squares commonly used in regression analysis is an unbiased estimation using the following formula:

$$\beta = (X^T X)^{-1} X^T y \quad (1)$$

where $X^T X$ is not the full rank and the determinant of $X^T X$ is close to 0. For a well posed problem, X is usually column full rank in which case $X\beta = y$. The calculation bias is large and the least squares estimate coefficient has instability problems, lacking stability and reliability. In order to solve the above problems, we added a small constant value of λ on the diagonal elements of matrix $X^T X$ in the formula:

$$\beta(\lambda) = (X^T X + \lambda I)^{-1} X^T y \quad (2)$$

In the above formula, I is the identity matrix. When the ridge parameter λ increases, the ridge regression coefficient β tends to 0. The path that β follows with the change of λ is called a ridge trace. In the actual calculation, many λ values can be chosen. When the ridge trace becomes stable, then the value of λ is selected. This is the ridge regression model.

The specific operation method of temporal interpolation was as follows: (1) we chose the station with the longest observation record as the main sta-

tion for Wuhan. (2) The time zone of the main station was identified, the ridge regression model was established by using the same hourly data for T_{max} (T_{min}) as the main sequence station during 1961–1978. The data from the modern stations from 1961 to 1978 were selected in order to avoid the impact of regional socio-economic activities and global changes after China started to reform and open up in 1978. Use of the data from before 1978 avoids the impact of urbanization on temperature as much as possible, and keeps good consistency with the early temperature data, which should further improve the fitting effect of the model. (3) The fitting equation expression obtained from 2 sets of data was substituted into the early data for the missing T_{max} (T_{min}), and the early missing T_{max} (T_{min}) data was interpolated.

As temperature change has obvious seasonality, the station data was divided into 12 months. The 12 month extreme temperature data were divided into a training set and a test set according to the ratio of 7:3. Machine learning was used to obtain the relationship between T_{max} (T_{min}) and hourly data in each month. The optimal learning model for each month at the different stations was determined by setting different random seeds.

After temporal interpolation, merging the modern and the early-period data, we finally established the T_{max} and T_{min} of Wuhan during 1881–2020.

2.2.2. Cross-validation of interpolation methods

In order to verify the credibility of the regression model, a case study was conducted (Fig. 3) taking Station 1901208 as an example, which had an observation period from 1936 to 1937. From a total of 670 days, 335 had no missing records for T_{max} and T_{min}, and these days were basically continuous within a year. Therefore, we could regard the T_{max} and T_{min} data of these 335 days as unknown, and then compare the predicted values obtained from the regression model to the actual values to assess the prediction effect of the model. As can be seen in Fig. 3, the differences between the predicted values and the actual values were not large. The sample size was 335, the mean square error (MSE) of the maximum value was 2.02, the root mean squared error (RMSE) was 1.42, the mean absolute error (MAE) was 1.09, and the correlation coefficient between predicted and actual values was 0.38, which passed the confidence level test at 99.99%. The MSE of the minimum value was 0.96, the RMSE was 0.98, the MAE was 0.72, and the correlation coefficient between predicted and actual values was 0.44, which also passed the confidence level test at 99.99%. Therefore, the reliability of the interpolation results is very high and convincing. It is worth noting that the temperature forecast on certain days was poor, mainly because this is a pure mathematical model that does not fully consider other meteorological factors affecting the temperature.

2.3. Homogenization

The RHtestV4 software developed by Wang & Feng (2013) was used to test and adjust the inhomogeneity of daily temperature data. High-quality reference series were constructed for comparing the target series; the data for these were collected from the Berkeley Earth merged dataset, version 2 (Rohde et al. 2013), which is a composite collection of more than 10 sets of temperature datasets.

The reference series were tested and determined according to the following steps: Firstly, taking the target station as the center, the reference stations within a radius of 500 km were selected, ensuring that the altitude difference between the reference station and the target station was less than 200 m. Then, the correlation coefficient between the first-order target station series and the first-order reference station series was calculated, and the reference station series with correlation coefficients of >0.8 were selected. Because the RHtest uses only 1 reference series to test the homogeneity of the target station series, obvious breakpoints in the reference series are likely to introduce additional inhomogeneity to the target series in the detection process. Therefore, the homogeneity of the selected reference station series was preliminarily tested without reference or metadata (to avoid a too complex process and overlong computation time). In this way, reference station series that contained significant breakpoints were discarded, and the average of 5 homogeneous reference station series was used to test the inhomogeneity of target station series.

Squares of the correlation coefficients between the reference and target station series were taken as weights to form averaged reference series using the weighted average method. The homogeneity of the averaged reference series was then tested again, and the results showed that the averaged reference series for T_{max} and T_{min} were both homogeneous (Fig. 4). For all of the tests, the confidence level was set to

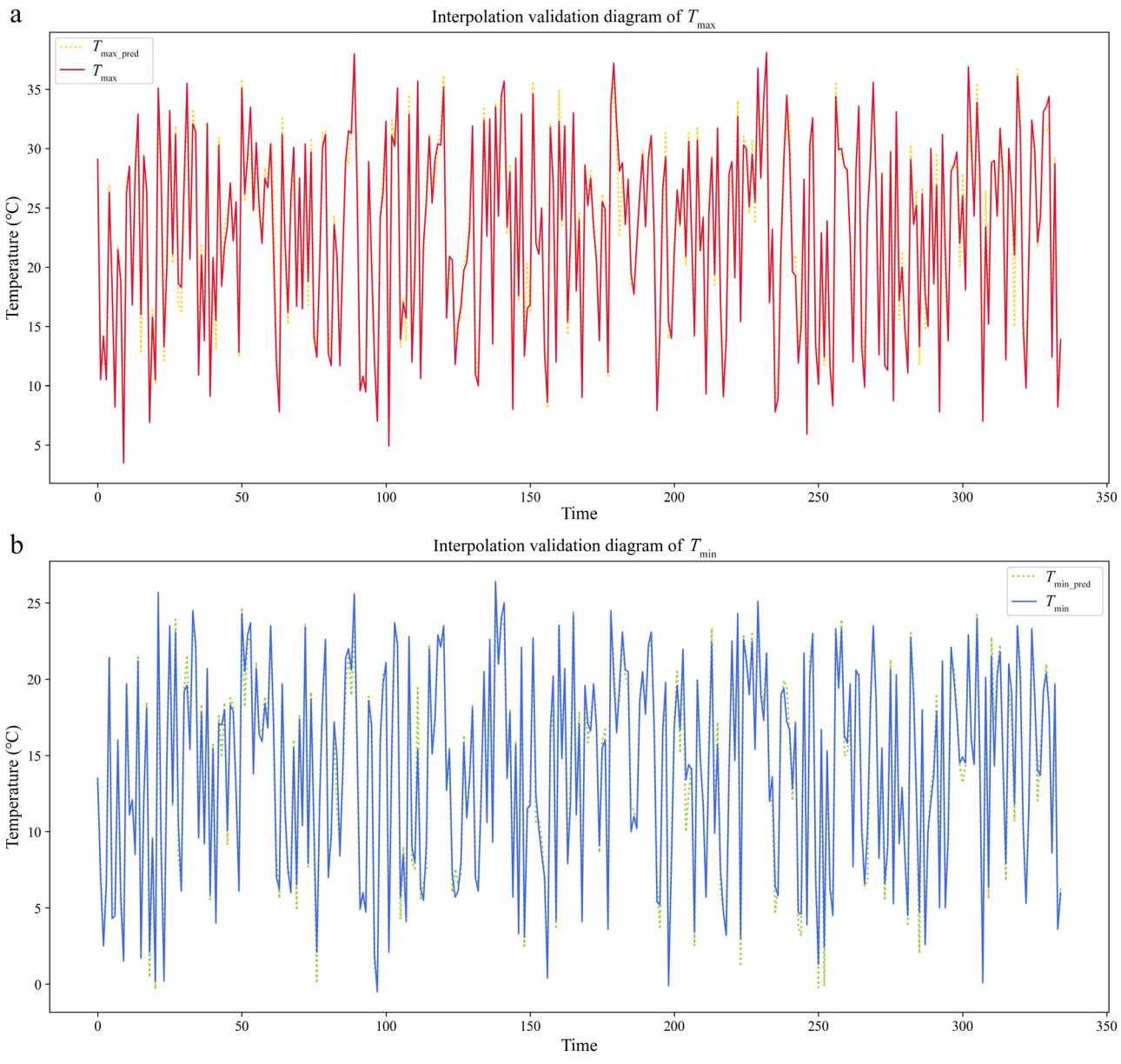

Fig. 3. Comparison between predicted and actual temperature values for Station 1901208

99.99% to ensure the recognized breakpoints were the most significant.

For accuracy reasons, the detection was first conducted on the monthly data that was converted from daily data. Then, the quantile matching (QM) method (Vincent et al. 2012) was used to adjust the daily temperature data according to the detection results. In order to reduce the uncertainty during the adjustment as much as possible, and to avoid the adjustment of too many unnecessary breakpoints (which may result from local climatic variabilities, rather than non-climatic factors), the adjustment values of the breakpoints were limited. The average of the highest daily temperature and lowest daily temperature in every year of the target station series were taken as the upper and lower bounds of the threshold. If the absolute values of the adjustments were neither larger than 1/30 of the difference between the upper and lower thresholds, nor supported by any metadata, the breakpoints were not adjusted. As a result, the original characteristics of the series was retained to avoid false adjustments of possible climatic variabilities. The detailed breakpoint detection results and adjustment values are shown in Table 2.

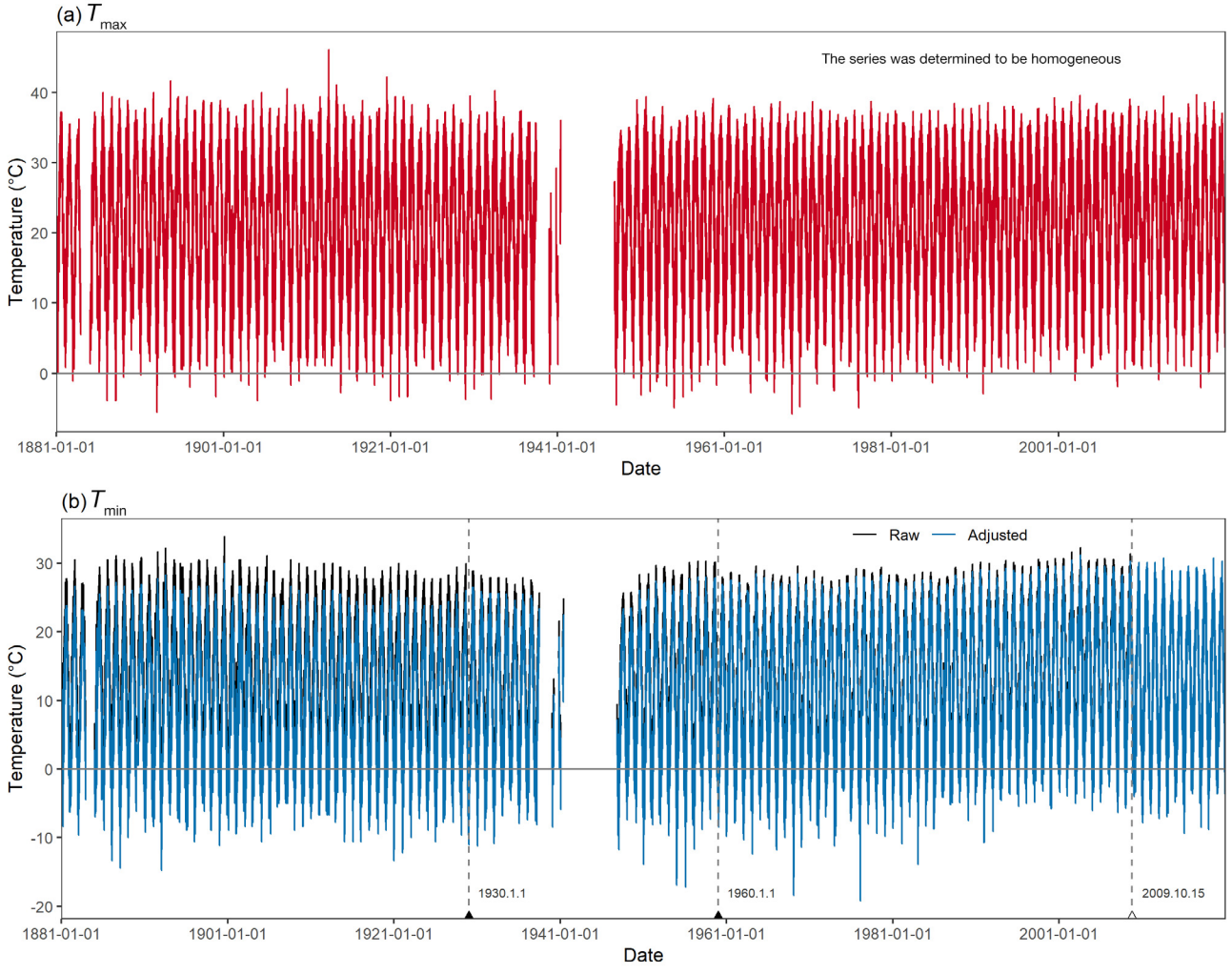

Fig. 4. The daily temperature series of (a) T_{max} and (b) T_{min} in Wuhan from 1881 to 2020. The T_{max} series was determined to be homogeneous under the 99.99% confidence level. The T_{min} series contains 3 breakpoints on 1 January 1930, 1 January 1960, and 15 October 2009 (vertical dashed lines). The former 2 breakpoints correspond to data interpolation and station relocation, respectively (i.e. supported by metadata, solid triangles). The last breakpoint lacks metadata support, but is significant under the 99.99% confidence level (hollow triangle). The temperature value of 0°C is indicated (solid horizontal line)

Table 2. Detection and adjustment of breakpoints in T_{max} and T_{min}

Data	Breakpoint date (yr/mo)	Average adjustment (°C)	Metadata	Exceeds the adjustment threshold	Adjustment decision
T_{max}	1915/11	−0.85	No support	No	Discarded
	1996/12	0.51	No support	No	Discarded
T_{min}	1930/01	−2.56	Data interpolation	—	Adjusted
	1960/01	−0.42	Station relocation	—	Adjusted
	1989/09	0.67	No support	No	Discarded
	1995/01	0.87	No support	No	Discarded
	2009/10	−1.26	No support	Yes	Adjusted[a]

[a]As 1/30 of the difference between the upper and lower thresholds for T_{max} and T_{min} is 1.26°C and 1.17°C, respectively, the T_{min} breakpoint in October 2009 was adjusted even without metadata support

2.4. Extreme high temperature indices

Based on the homogenized T_{max} and T_{min} temperature data obtained through the above steps, this study analyzed the temporal changes of several extreme temperature indices. Specifically, 26 extreme high temperature indices were employed to analyze the long-term extreme climate change in Wuhan. Some of these indices refer to the extreme indices defined by the Expert Team on Climate Change Detection and Indices (ETCCDI) (http://etccdi.pacificclimate.org/list_27_indices.shtml), including the extreme value indices (annual maximum value of daily T_{max}, TXx; annual maximum value of daily T_{min}, TNx) and the relative threshold indices (percentage of days when T_{max} > 90th percentile, TX90p; percentage of days when T_{min} > 90th percentile, TN90p). Additionally, extreme high temperature indices with different absolute temperature thresholds are defined based on Wuhan's weather and climatic features to examine weather and climatic changes under distinct extreme circumstances. It is worth noting that both average temperature (T_{ave}), which is the arithmetic mean of daily T_{max} and T_{min}, and DTR, which is the difference between daily T_{max} and T_{min}, are also considered extreme temperature indices since they are derived from the extremes of daily T_{max} and T_{min}. Detailed definitions of the indices are provided in Table 3.

2.5. Trend estimation methods

Most of the extreme temperature index series do not obey normal distribution, as found by using the Shapiro-Wilk normality test. It is thus not reasonable to use the least squares method to estimate the long-term trend (Zhang et al. 2004). In this study, the nonparametric Theil-Sen trend estimation method was used, and the Mann-Kendall method was used to test the trend significance (Mann 1945, Sen 1968).

It is calculated by the following steps:

First construct the test statistic S:

$$S = \sum_{i=1}^{n-1} \sum_{j=i+1} \mathrm{sign}(X_j - X_i) \quad (3)$$

Based on the test statistic S, construct the test statistic Z:

Table 3. Definitions of extreme temperature indices used in this study. ETCCDI: Expert Team on Climate Change Detection and Indices

Index type	Index name	Definition	Unit
Extreme temperature (indices)	T_{max}	Daily maximum temperature	°C
	T_{min}	Daily minimum temperature	°C
	T_{ave}	Average value of daily T_{max} and T_{min}	°C
	DTR	Difference between daily T_{max} and T_{min}	°C
ETCCDI-defined indices	TXx	Annual maximum value of daily T_{max}	°C
	TNx	Annual maximum value of daily T_{min}	°C
	TX90p	Percentage of days when T_{max} > 90th percentile	%
	TN90p	Percentage of days when T_{min} > 90th percentile	%
Newly defined absolute threshold indices	TX35	Annual count when daily T_{max} > 35°C	d
	TX38	Annual count when daily T_{max} > 38°C	d
	TX40	Annual count when daily T_{max} > 40°C	d
	TN25	Annual count when daily T_{min} > 25°C	d
	TN28	Annual count when daily T_{min} > 28°C	d
	TN30	Annual count when daily T_{min} > 30°C	d
	TX35c	Annual count when daily T_{max} > 35°C continuously	d
	TX38c	Annual count when daily T_{max} > 38°C continuously	d
	TX40c	Annual count when daily T_{max} > 40°C continuously	d
	TN25c	Annual count when daily T_{min} > 25°C continuously	d
	TN28c	Annual count when daily T_{min} > 28°C continuously	d
	TN30c	Annual count when daily T_{min} > 30°C continuously	d
	TX35Mc	Maximum TX35c in a year	d
	TX38Mc	Maximum TX38c in a year	d
	TX40Mc	Maximum TX40c in a year	d
	TN25Mc	Maximum TN25c in a year	d
	TN28Mc	Maximum TN28c in a year	d
	TN30Mc	Maximum TN30c in a year	d

$$Z = \begin{cases} \dfrac{(S-1)}{\sqrt{\dfrac{n(n-1)(2n+5)}{18}}} & S > 0 \\ 0 & S = 0 \\ \dfrac{(S+1)}{\sqrt{\dfrac{n(n-1)(2n+5)}{18}}} & S < 0 \end{cases} \quad (4)$$

where $Z > 0$, indicates an increasing trend and $Z < 0$ indicates a decreasing trend.

The magnitude of the trend is measured using Sen's slope β:

$$\beta = \text{median}\left(\frac{X_j - X_i}{i-j}\right) \quad \forall j < i \quad (5)$$

where $\beta > 0$ indicates an upward trend and $\beta < 0$ indicates a downward trend. A p-value corresponding to β was used to determine whether the trend is significant, with $p \leq 0.05$ (0.01) indicating significance.

3. RESULTS

This section primarily analyzes the temporal characteristics of extreme temperatures (T_{max}, T_{min}, T_{ave}), extreme value indices (TXx, TNx), relative threshold indices (TX90p, TN90p), DTR, and operationally applied indices in Wuhan. Furthermore, an assessment of the changing trends of each index during different periods is presented.

3.1. Extreme and average temperatures

Fig. 5 displays the annual mean time series and decadal box plots of T_{max}, T_{min}, and T_{ave} in Wuhan from 1881 to 2020. The T_{max} warming trend did not show statistical significance throughout the 140 yr period. Prior to 1910, there was an apparent decreasing trend, followed by a sharp increase that peaked

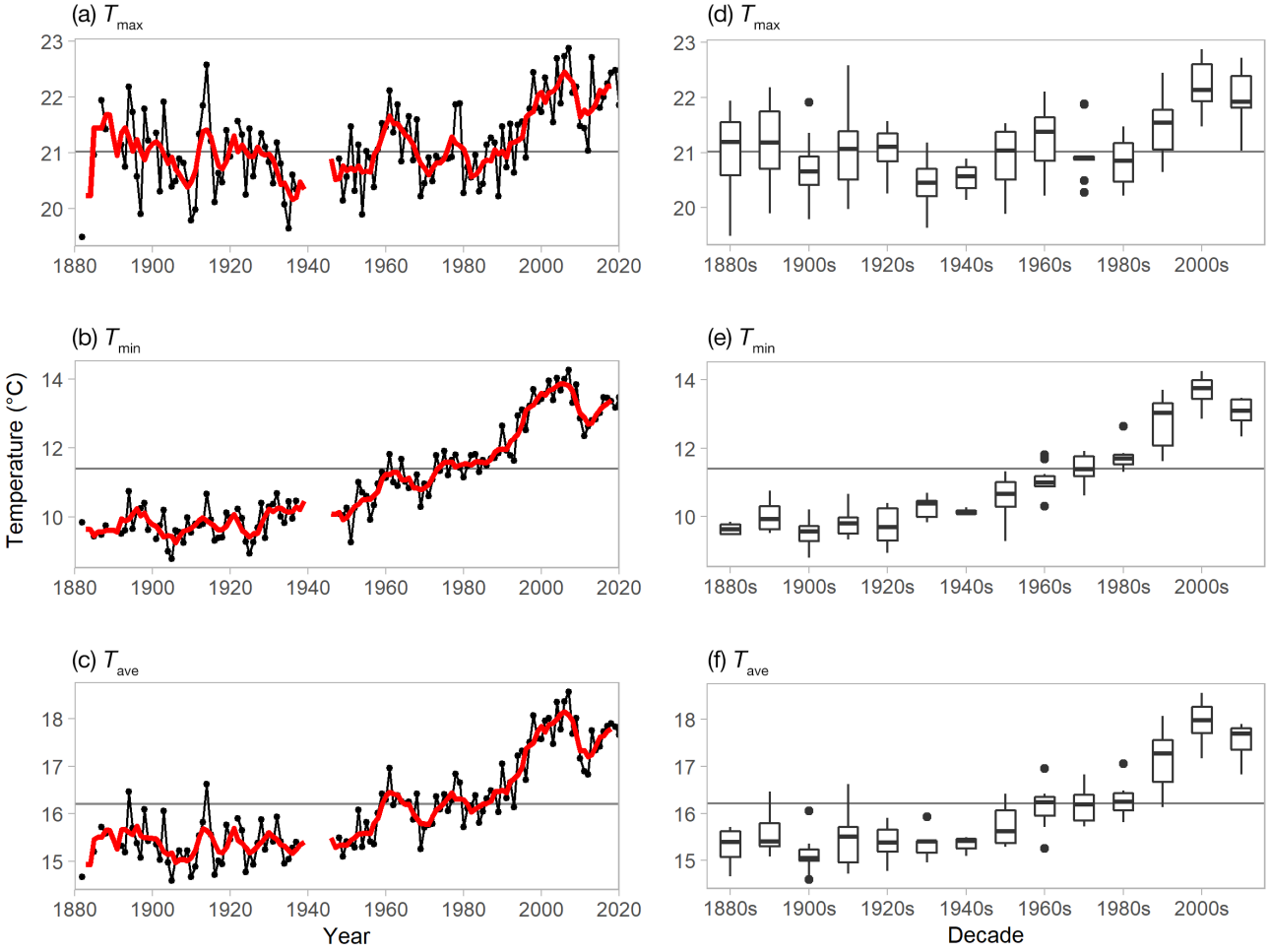

Fig. 5. (a,b,c) Annual and (d,e,f) decadal series for T_{max}, T_{min}, and T_{ave} in Wuhan from 1881 to 2020. Black horizontal line: mean value of the climate reference from 1961 to 1990; red curves in (a,b,c): 5 yr moving average; boxplots in (d,e,f) — horizontal bar in box: median; top and bottom of box: 1st and 3rd quartiles; whiskers: ≤1.5x the interquartile range; dots: outliers

during the first half of the study period in 1914. Another significant declining trend occurred for T_{max} from 1914 to 1935. Between 1935 and 1980, T_{max} fluctuated with flat trends before sharply rising. The primary warming period for T_{max} occurred roughly between 1980 and 2007, and the highest historical temperature recorded occurred in 2007 (Fig. 5a). Strongly positive anomaly decades were the 1890s and 1960s, corresponding to 2 peak anomalies. The most significant positive anomalies were distributed in the 2000s, the period with the highest observed temperature (Fig. 5d). On the other hand, T_{min} exhibited a more dramatic warming trend compared to T_{max}: it showed a pronounced upward trend from 1951 onward, while trends before 1951 remained relatively flat (Fig. 5b). From the inter-decadal changes, it is evident that T_{min} had a sustained and consistent warming trend from the 1880s to the 2000s. Additionally, the annual and inter-decadal variabilities of T_{min} were significantly smaller than those of T_{max} throughout the entire study period (Fig. 5e). There was no clear warming trend for T_{ave} before 1949, and the annual variability was moderately high, while inter-decadal variability exhibited wave-like patterns. From 1949 to 1961, T_{ave} increased rapidly, then decreased notably in the 1960s, forming a small peak in 1961. Since 1969, there has been a significant upward trend overall (Fig. 5c). It should be noted that T_{max}, T_{min}, and T_{ave} went through a sharp decline from 2007 to 2012, possibly reflecting the regional climate response to the global warming hiatus.

3.2. The ETCCDI indices and DTR

Fig. 6 depicts the variations in extreme value indices (TXx, TNx), relative threshold indices (TX90p,

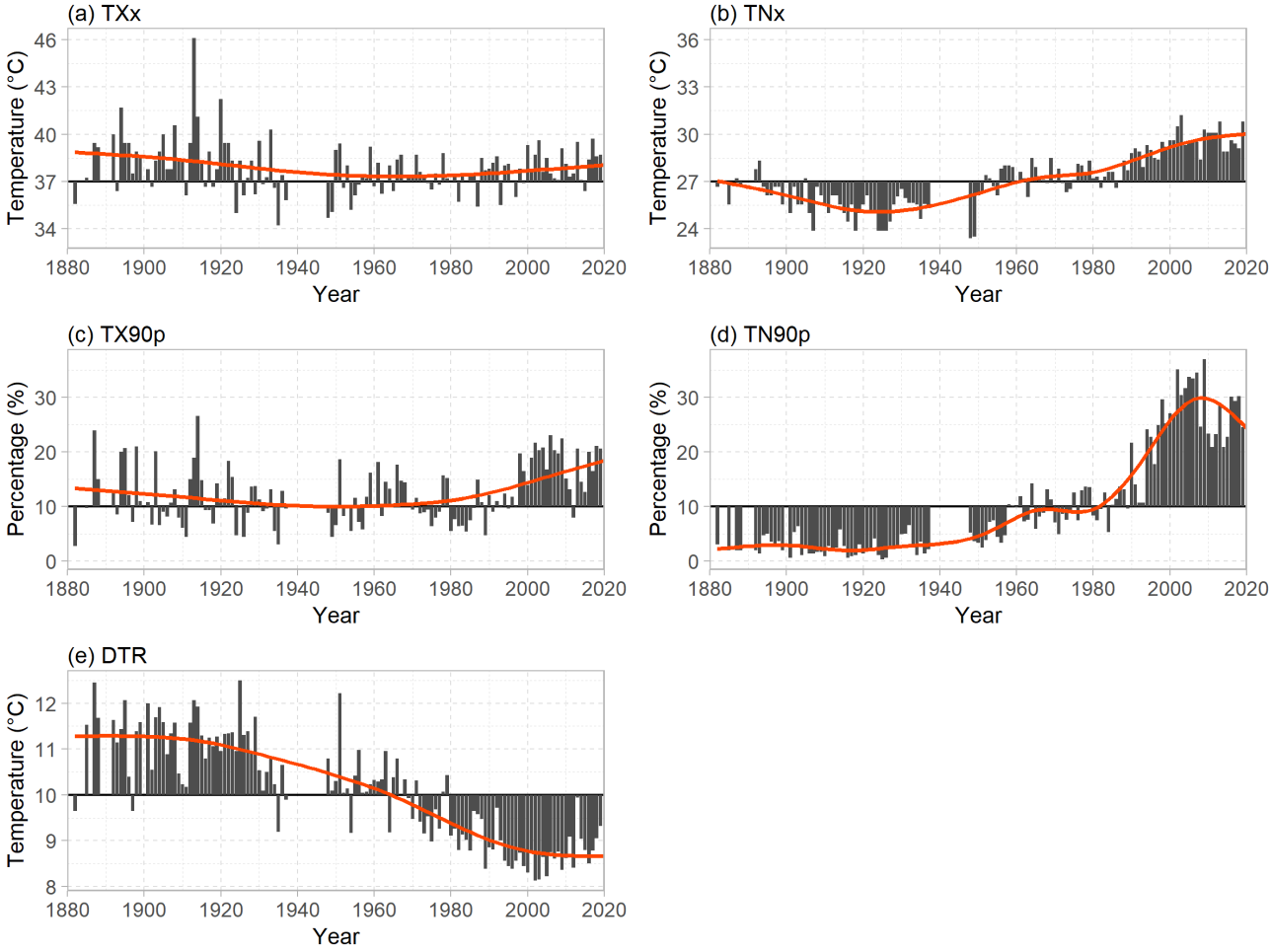

Fig. 6. Annual time series of extreme value indices: (a) TXx, (b) TNx; relative threshold indices: (c) TX90p, (d) TN90p; and extreme temperature index: (e) DTR; 1881 to 2020. Black horizontal line: mean value of the climate reference from 1961 to 1990; red curve: fit of the generalized additive model

TN90p), and DTR for Wuhan from 1881 to 2020. The highest historical peak value for TXx was around 46°C in 1913, indicating that the most severe high-temperature event recorded in Wuhan's history occurred during that year. During the study period, TXx displayed a gradual but insignificant downward trend (Fig. 6a). Meanwhile, TNx exhibited an opposite pattern before and after 1925, with a significant decrease from 1881 to 1925, followed by a substantial increase, reaching its highest value in 2003. There were apparent low-temperature anomalies in 1948 and 1949 within this period (Fig. 6b). The overall trend change for TX90p gradually decreased before the 1940s, then increased after the 1940s, resulting in no observable trend over the entire study period (Fig. 6c). The values of TN90p before the 1940s were below the average climate state, and maintained a stable level of trend change. It gradually increased after the 1940s, especially during the period from 1980 to 2009, when it increased sharply and reached a historical maximum in 2009. TN90p declined significantly in the 2010s, which could be related to the global warming hiatus (Fig. 6d). DTR conspicuously declined throughout the study period, with the most notable drop occurring between 1951 and 2000. Only a slight increase was observed after 2000 (Fig. 6e).

3.3. Absolute threshold indices

In Fig. 7, the series of extreme temperature indices under different thresholds reveal that in Wuhan over the past 140 years, most of the years (60 %) have had at least 15 days where the maximum temperature surpassed 35°C, and a substantial number of years (22 %) have experienced at least 1 month with temperatures exceeding 35°C. In 1894 and 1914, the number of days with temperatures surpassing 35°C even exceeded 50. Examining the time series, the an-

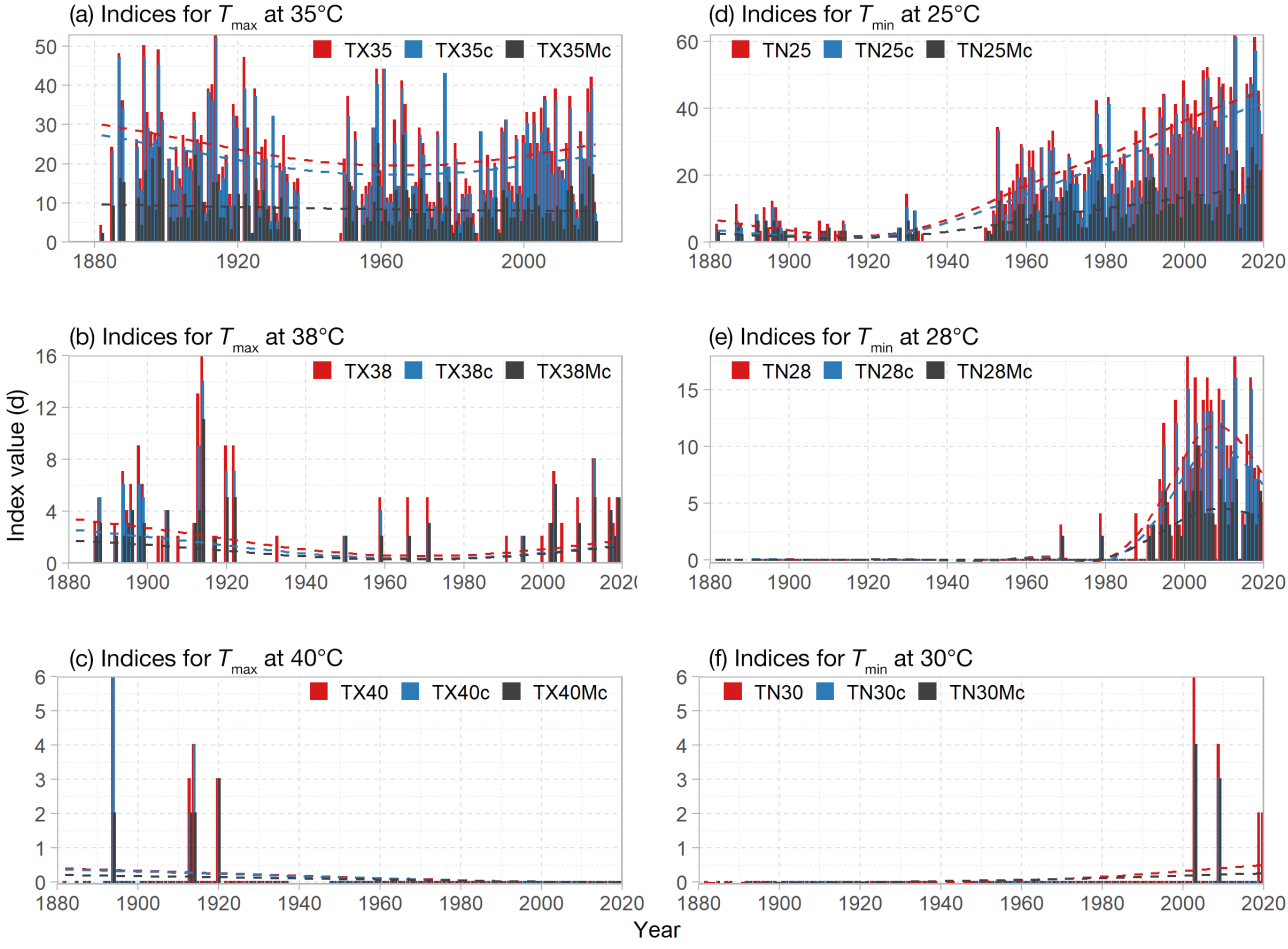

Fig. 7. The annual time series of indices at the (a) 35°C threshold, (b) 38°C threshold, and (c) 40°C threshold for T_{max}, and at the (d) 25°C threshold, (e) 28°C threshold, and (f) 30°C threshold for T_{min}. Dashed curves: fit of the generalized additive model

nual count of days with T_{max} above 35°C (TX35) was highest during the early study years but has dwindled in the last 30 to 40 yr. Overall, the number of extreme high-temperature days with T_{max} above 35°C gradually decreased. The TX35 index also indicates multiple inter-decadal cyclic variations, with 3 conspicuous troughs occurring in 1900, 1940, and 1980. This demonstrates that the TX35 index mainly occurred as a multi-decadal cyclical variation, with a period of approximately 40 yr. The changes in the annual count of days when T_{max} was continuously over 35°C (TX35c) and the maximum TX35c in a year (TX35Mc) agree with that of TX35, exhibiting multi-year and inter-decadal cyclic fluctuations. The value of TX35c was slightly smaller than that of TX35, which implies that days with extreme high-temperatures above 35°C generally occurred consecutively. During the study period, about 28% of the days had a T_{max} above 35°C for at least 10 continuous days (Fig. 7a). For the number of days with temperatures surpassing 38°C there was a significant drop from the early study years, with TX38 mainly occurring before 1920, reaching its historical peak in 1913 and 1914. Although there was an upward trend in days with extreme high-temperatures exceeding 38°C in Wuhan in the last 30 yr, the number is still significantly lower than it was during the early study period (Fig. 7b). There have only been a handful of incidents where T_{max} surpassed 40°C in Wuhan during the past 140 yr, with records of T_{max} above 40°C only occurring in 1894, 1913, 1914, and 1920 (Fig. 7c).

Regarding T_{min} (Fig. 7d), the frequency of extreme high-temperature events exceeding 25°C (TN25) was relatively low before the 1940s. However, beginning in the 1950s, there was a noticeable increase in such events, leading to a significant rise in the TN25 indices. Notably, the annual count of days when T_{min} was continuously over 25°C (TN25c) exhibited nearly identical changes to TN25, whereas the upward trend of maximum TN25c in a year (TN25Mc) was significantly lower than that of the latter two extreme indices after the 1950s. This increase in extreme high-temperature days surpassing the 25°C threshold over the past 70 yr appears to be primarily continuous. While the maximum duration of these events has also lengthened, the increase in duration lags considerably behind that of the overall rise in extreme high-temperature days, indicating that shorter-duration events are becoming more frequent. Extreme high-temperature events with a T_{min} exceeding 28°C have almost exclusively occurred in the past 30 years, with a sharp rise observed from the 1990s to the 2000s and culminating in a pronounced peak in the latter decade (Fig. 7e). Extreme high-temperature events with a minimum temperature of over 30°C were rarely observed, the only records of such events occurred in 4 years: 2003, 2009, 2019, and 2020 (Fig. 7f).

3.4. Monthly temperature changes

Fig. 8 displays monthly anomaly heatmaps of T_{max}, T_{min}, and T_{ave} from 1881 to 2020. The temperature anomaly of T_{max} showed no significant trend or difference throughout the study period, with only a slight increase observed in the last 20 yr and the most evident positive anomalies occurring between February and May. Between 1881 and 1911, the anomaly values were primarily negative from January to April, indicating that the period from January to May showed the greatest temperature trend for T_{max} over the study period. However, the temperature from June to December only showed relatively clear positive anomalies in the early period (1885–1901) (Fig. 8a). In contrast, the variation in the anomaly heatmap for T_{min} was more pronounced, with temperatures generally displaying negative anomalies before 1981 and positive anomalies afterward, indicating a substantial warming trend in each month. Between 1881 and 1931, almost all monthly temperatures from February to August showed significant negative anomalies, whereas in the last 30 yr, temperatures for almost all months exhibited significant positive anomalies, especially from February to August, contributing strongly to the overall T_{min} trend (Fig. 8b). Similar to T_{min}, the anomaly of T_{ave} exhibited generally negative values before 1981 and generally positive values afterward, but the absolute values of the anomalies are smaller than those of T_{min}. The period from February to July had the most temperature changes for T_{ave}, where the anomalies were predominantly negative between 1881 and 1911, and overwhelmingly positive between 1991 and 2020, which were 2 of the most anomalous periods for T_{ave} over the study period. However, the temperature trend from August to January showed less variation (Fig. 8c).

3.5. Changes in monthly extreme indices

Fig. 9 illustrates the heatmaps of the extreme value indices (TXx, TNx), relative threshold indices (TX90p, TN90p), and DTR anomalies. Positive anom-

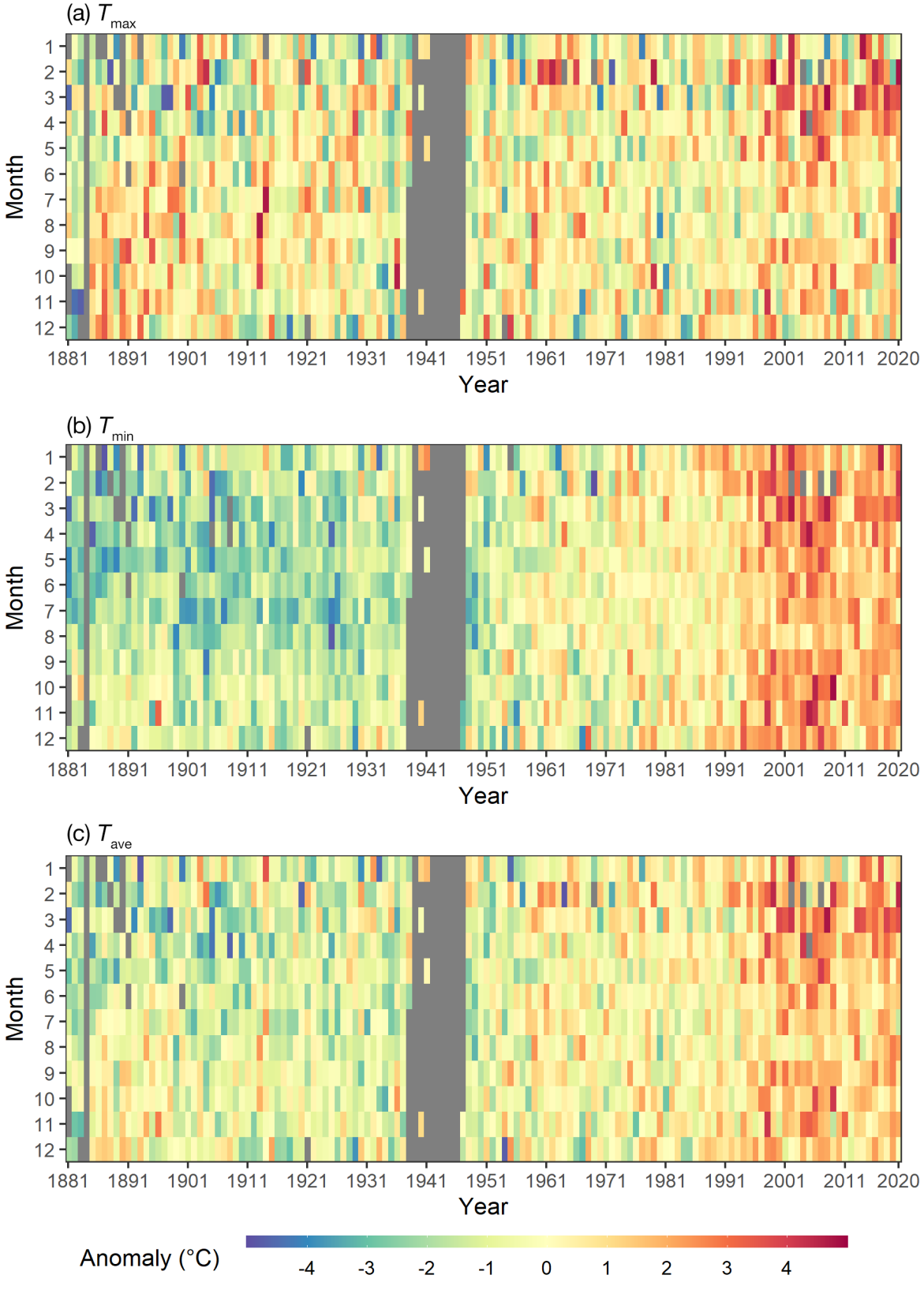

Fig. 8. The monthly anomalies of (a) T_{max}, (b) T_{min}, and (c) T_{ave} from 1881 to 2020. The anomalies were calculated with reference to the climate period from 1961 to 1990. Grey shading: months with missing values

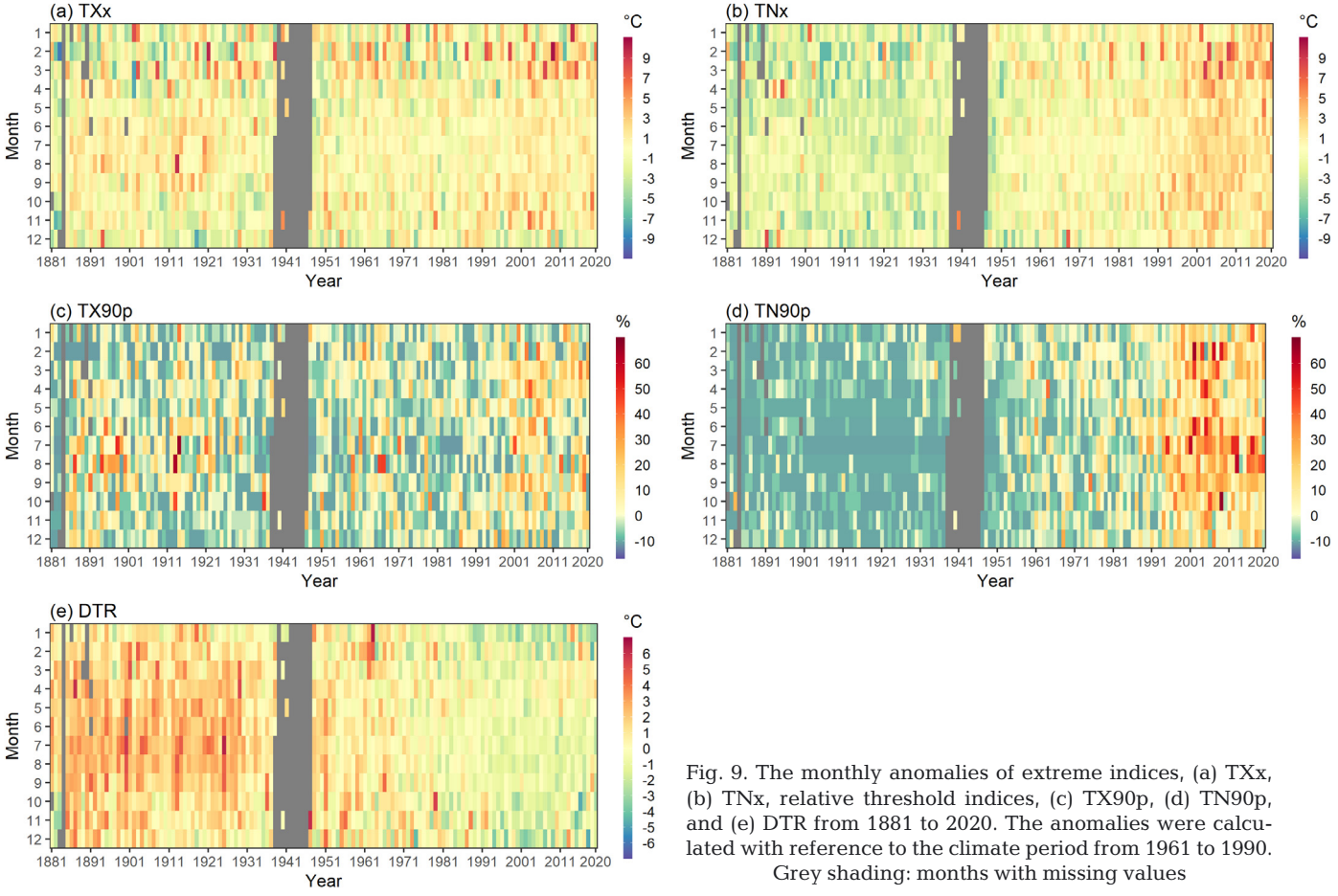

Fig. 9. The monthly anomalies of extreme indices, (a) TXx, (b) TNx, relative threshold indices, (c) TX90p, (d) TN90p, and (e) DTR from 1881 to 2020. The anomalies were calculated with reference to the climate period from 1961 to 1990. Grey shading: months with missing values

alies dominated for TXx during the study period, although no significant temporal trend was evident overall. One notable observation was that the months from February to April showed the most marked changes, with March displaying a distinct 20 yr cyclic inter-decadal variation in anomalies (Fig. 9a). For TNx, the anomalies had relatively more pronounced changes, which could be divided into 3 parts: negative anomalies before 1951, near zero anomalies between 1951 and 1991, and positive anomalies after 1991. As a result, TNx exhibited an upward trend in all months throughout the study period, with the most significant increase occurring between February and April (Fig. 9b). The distribution of anomalies for TX90p was uniform between positive and negative in general, with no clear changing tendencies. Nonetheless, it had slightly higher-than-average (positive) anomalies during the two 20 yr periods at the beginning and end of the study period, from April to December and from March to September, respectively (Fig. 9c). TN90p showed similar distributions to TNx and could also be categorized into 3 parts spanning the study period: consistently negative anomalies before 1951, oscillating positive and negative values with a mean near zero between 1951 and 1991, and markedly positive anomalies after 1991. As a result, TN90p exhibited a significant and consistent upward trend throughout the study period (Fig. 9d). DTR anomalies showed a positive-to-negative transition in the 1970s, with predominantly positive anomalies before this period and mostly negative anomalies after it, resulting in a significant downward trend in DTR across all months throughout the study period (Fig. 9e).

The changing characteristics of the anomalies of these 5 extreme temperature indices reflect a pronounced asymmetric trend between T_{max} and T_{min}. Indices associated with T_{max} (i.e. TXx and TX90p) did not exhibit significant temporal changes, while those associated with T_{min} (i.e. TNx and TN90p) showed noticeable upward trends. This asymmetric feature is particularly evident in DTR, where positive anomalies were present during the first 100 yr of the study period, while negative anomalies dominated during the latest 40 yr, indicating a more significant increase in T_{min} than T_{max}.

3.6. Long-term trends of different periods

The study period was divided into 2 sub-periods, 1881–1940 and 1951–2020, based on variations in the observed temperature indices over different periods. Table 4 demonstrates the trends in various temperature indices over time for these sub-periods, excluding the 1940s due to missing values. Trends during the first sub-period were mostly insignificant, whereas most indices during the second sub-period demonstrated significant trends passing the 0.05 significance test, where positive trends dominated. These findings may indicate Wuhan's urbanization over the last 70 yr. Although extreme temperature events were rare in most periods (identified in Table 4), some indices displayed evident changes. For example, changes in the extreme high-temperature days with T_{min} over the 25°C threshold were noticeable during both sub-periods and the entire study period. The extreme high-temperature days with T_{max} over the 35°C threshold showed a significant downward trend during the first sub-period, but increased rapidly during the second sub-period. Therefore, significant changes in temperature extremes have occurred in Wuhan under these 2 threshold indices. Even though such extreme events showed a reduction in the early stages of the study period, they have significantly increased in the past 70 yr, particularly extreme high-temperature events for T_{min}.

Table 4. Trends of indices in different periods. **Bold**: significant values ($p < 0.05$)

Indices	1881–1940	1951–2020	1881–2020	Unit (dec^{-1})
T_{max}	−0.11	**0.21**	**0.08**	°C
T_{min}	0.08	**0.49**	**0.32**	°C
T_{ave}	0	**0.35**	**0.2**	°C
TXx	−0.35	**0.15**	−0.04	°C
TNx	**−0.32**	**0.5**	**0.37**	°C
TX90p	−0.74	**1.21**	**0.34**	%
TN90p	0	**3.86**	**1.78**	%
DTR	**−0.18**	**−0.3**	**−0.26**	°C
TX35	**−2.69**	0.97	−0.34	d
TX38	**0**	**0**[a]	0[a]	d
TX40	0[a]	0[a]	**0**[a]	d
TN25	**−0.29**	**4.72**	**3.37**	d
TN28	0[a]	**1.25**[a]	**0**[a]	d
TN30	0[a]	**0**[a]	**0**[a]	d
TX35c	**−2.97**	0.88	−0.31	d
TX38c	0[a]	**0**[a]	0[a]	d
TX40c	0[a]	0[a]	**0**[a]	d
TN25c	0[a]	**4.57**	**3.1**	d
TN28c	0[a]	**0.83**[a]	**0**[a]	d
TN30c	0[a]	**0**[a]	**0**[a]	d
TX35Mc	**−1.15**	0.23	0	d
TX38Mc	**0**[a]	**0**[a]	0[a]	d
TX40Mc	0[a]	0[a]	**0**[a]	d
TN25Mc	**0**[a]	**1.43**	**1.09**	d
TN28Mc	0[a]	**0.54**[a]	**0**[a]	d
TN30Mc	0[a]	**0**[a]	**0**[a]	d

[a]Proportion of 0 values during the corresponding period exceeds 50%

4. DISCUSSION

4.1. Observed trends

The above results indicate that Wuhan has significantly warmed since the 1950s, and especially since the 1970s. After 1951, the warming rate of T_{max} in Wuhan obtained in this study was 0.21°C per decade (dec^{-1}), and the warming rate of T_{min} was 0.49°C dec^{-1}. These results are slightly higher than those of a previous study using similar time periods (Yao et al. 2010), but overall they are relatively consistent. According to the Hubei Province Climate Change Bulletin (Hubei Meteorological Bureau 2018), the annual mean temperature in Wuhan showed a significant increasing trend from 1951 to 2018, with a warming rate of 0.30°C dec^{-1}. In comparison, the obtained warming rate of T_{ave} during the same period in this study was 0.05°C dec^{-1} higher. Overall, the temperature trend for Wuhan in this study appears to be slightly higher than that of previous studies, mainly reflected in T_{min} and T_{ave}. The slightly higher warming rate than those of previous analyses may be related to the different time periods, different averaging methods for daily mean temperature, and different methods for homogenization of the temperature data applied in the studies.

In general, Wuhan has warmed significantly since the early 1950s. Over the last 60 yr or more, extreme high temperatures occurred more frequently, though some rare extreme high temperature events happened less frequently than in the early period. Unlike the significant increase in average temperature, the rising trends of extreme high temperature in Wuhan were weak in recent decades, but the proportion of extreme high temperature days increased significantly compared to the previous period. Therefore, the warming in the last 140 yr in terms of extreme temperature events mainly occurred during the last half century. However, Wuhan experienced more extreme high temperature events in the early period, e.g. T_{ave}, TN90p, and TX90p peaked in 1914, and

the maximum TXx reached 46.1°C in 1913, which is the highest temperature in the reconstructed T_{max} data.

It was also found that the temperature trends in Wuhan in the early period were opposite to those in recent decades, and almost all the indices showed a cooling trend in the early period. The opposite trends of temperature change before and after the 1940s shown in this analysis were also found in other studies. Yan et al. (2017) reported that 2 warm periods were experienced during 1906–1946 and 1994–2015 in Wuhan; and between 1947 and 1993, annual mean temperature was relatively low. This result is partially consistent with our research, and the obtained T_{max} in this study also exhibited roughly 3 multidecadal fluctuations of 'warm-cold-warm' in Wuhan. However, T_{min} and T_{ave} did not show similar prominent variations, as our homogenization reduced the overall temperature of the subseries before the breakpoint, causing T_{min} and T_{ave} to show a more consistent warming trend. The higher estimate of warming trend after homogenization may be related to the homogenization of the breakpoints caused by relocation of the observation stations (Zhang et al. 2014, Ren et al. 2015).

The maximum and minimum temperatures, and the resulting extreme temperature indices, in Yingkou in Northeast China also showed different changes before and after 1950, with the DTR exhibiting an opposite trend in the early and recent periods (Xue et al. 2021). The study by Sun et al. (2021) indicated that the 2-stage changes in T_{max}, T_{min}, and DTR during the last 120 yr have a universality in East Asia, and they may have been partially caused by the early-stage increase and recent decrease in cloudiness and precipitation in the region.

4.2. Limitations of data processing

A sufficiently long high-resolution temperature series was collected and analyzed in this study. However, the observation methods and the instruments were primitive before 1950, some records between 1940 and 1950 were unavailable, and the data was observed and recorded manually, so may contain errors to some degree. The main time series used in this study was formed by blending and interpolation of multiple single station series, which also hindered the matching of the early data to corresponding metadata in the process of homogenization. The data from before 1950 was mainly obtained from 9 different sites, which had independent historical data. However, since these sites no longer exist, making it laborious to collect and digitize corresponding early metadata records, it was difficult to verify the homogeneity of early data, which also increased the uncertainty of early data to some extent. Recovery and digitization of the missing records needs time, and to completely remove the data errors requires more in-depth quality control, homogenization, and verification. This will be done in our future studies.

As shown in Table 2, the inhomogeneity test identified 2 breakpoints for T_{max}. However, these breakpoints were discarded as they lacked metadata support and did not surpass the specified temperature threshold. Two unsupported breakpoints in T_{min} were similarly discarded. It should be noted that the temperature threshold used to determine whether unsupported breakpoints require adjustment is subjectively determined, with prior studies employing different thresholds based on specific research subjects (Cao et al. 2016, He et al. 2023). It is common for data homogenization to involve subjective factors in the process, which is critical for its success. Relying on fully automated computer programs for homogenization may be unreliable (Aguilar et al. 2003, Wang & Feng 2013). For this study, we set the threshold by calculating 1/30 of the average temperature difference between the highest daily temperature and the lowest daily temperature in all years. This criterion was based on multiple trials and comparisons of the diagnostic plots generated by the detection software. Regarding the temperature series of Wuhan Station, breakpoints that exceed this threshold were more prominent, while those below the threshold were more similar to local climate variations.

From the perspective of trend changes, the trend of adjusted T_{min} is slightly larger (+0.04°C dec^{-1}) than that of previous research (Yao et al. 2010). From the perspective of our data processing, the homogenization itself will have enlarged the trend of the adjusted series, which may be a consequence of the recovery of urbanization effects in the station temperature series due to the relocation from urban to rural areas (Zhang et al. 2014, Ren et al. 2015). Therefore, the adjusted series should contain a larger degree of urbanization effect, which needs to be assessed in future studies. A large and significant urbanization effect (bias) in annual and seasonal mean and extreme temperature data series has been affirmed in many previous studies (e.g. Chen et al. 2007, Ren et al. 2007, Ren & Zhou 2014, Tysa et al. 2019).

It is also worth noting that the statistical method employed to calculate the daily mean (monthly and annual mean) temperature may overestimate trends

in annual mean temperatures. In this study, the daily, monthly, and annual mean temperatures were obtained by calculating the arithmetical average of daily T_{max} and T_{min}. However, compared to the standard procedure or equal-interval averaging method (4, 8, 24 records a day), the arithmetic mean of T_{max} and T_{min} tends to overestimate the overall average and the linear trends, as pointed out by Liu et al. (2019). This may be related to the lightly higher upward trend in annual mean temperature in Wuhan. Therefore, it is imperative to take this factor into account in future studies.

4.3. Future work

In our study, attribution analysis of the long-term changes in the extreme high temperature indices was not performed. The significant warming observed in Wuhan during the past few decades can be attributed largely to an intensified 'urban heat island' effect, as demonstrated by Chen et al. (2007), Gui et al. (2019), and Jia et al. (2019). Previous analyses have indicated that urbanization accounts for 64.5% and 67.3% of the annual warming of T_{ave} and T_{min}, respectively, during the period of 1960–2000, and about 81.3% of the summertime warming between 1981 and 2000 (Chen et al. 2007, Ren et al. 2007). As a result, our identification of extreme temperature trends in Wuhan may be attributable, at least in part, to the effects of urbanization. Ren & Zhou (2014) found that the contribution of urbanization to urban maximum and minimum temperature extremes (TXx and TNx) averaged 22.7 and 26.1%, respectively, across Mainland China from 1961 to 2008. In addition, warm days and warm nights were affected by urbanization to the extent of 10.7 and 26.4%, respectively. Although urbanization in Wuhan has been concentrated in recent decades, the extent to which early temperature records were also impacted by urbanization remains unclear. With the steady progress of the Atmospheric Circulation Reconstruction over the Earth (ACRE) project (Allan et al. 2011), and other national research projects on early-period data recovery and digitization, more and more early data are being excavated and digitized. Thus, further effort is required to establish a reference series matching the same time scale as the urban series, so as to assess Wuhan's long-term urbanization effect thoroughly. Future research should also investigate the larger-scale factors driving extreme temperature changes in Wuhan.

5. CONCLUSIONS

Based on the newly integrated and extended daily temperature data of Wuhan station from 1881 to 2020, we employed 26 extreme temperature indices to analyze the variations and long-term changes in extreme high temperatures and events in Wuhan over the past 140 yr. The conclusions can be drawn as follows:

(1) Over the span of more than a century, Wuhan's maximum (T_{max}) and minimum (T_{min}) temperatures have shown discernable differences in terms of their patterns of variation. The annual and decadal fluctuations of T_{max} are quite significant and there is no clear evidence of an observable warming trend, with the most apparent increase occurring from 1980 to 2007. In contrast, T_{min} has undergone considerable warming, with a sustained overall upward trend (0.32°C dec^{-1}). Furthermore, the average temperature (T_{ave}) has risen significantly by 0.20°C dec^{-1} over the past 140 yr. Prior to 1960, there were no significant trends in T_{max}, T_{min}, and T_{ave}. Nonetheless, the most observable warming transpired during the past 40 to 60 yr. Moreover, there was a notable drop in both T_{max} and T_{min}, as well as T_{ave}, between 2007 and 2012; this may be linked to the global warming hiatus phenomenon.

(2) The extreme value indices (TXx, TNx) and the relative threshold indices (TX90p, TN90p) exhibited similar variation patterns. The indices pertaining to maximum temperature (TXx, TX90p) demonstrated a relatively stable trend over the past 140 yr with insignificant or slight declines. In contrast, the indices associated with minimum temperature (TNx, TN90p) have experienced significant changes in trends. Prior to 1980, the trends for TNx and TN90p were relatively stable or slightly increasing; however, they began to increase significantly after 1980. The DTR, on the other hand, demonstrated consistent behavior by continuously decreasing over the past century and a half.

(3) Over the past 140 yr, Wuhan has encountered frequent episodes of extreme heat. In many years, the maximum temperatures reached or exceeded 35°C for at least 15 days. However, in general, the number of extreme heat days with Tmax above 35°C has gradually decreased. The TX35 index series shows that these extreme heat days demonstrate multidecadal periodic variations of around 40 yr. Similarly, the TX35c and TX35Mc indices displayed identical time trends to those of the TX35 indices, suggesting that they too experience multidecadal periodic changes. While the number

of days with a maximum temperature exceeding 38°C markedly declined throughout the study period, they occurred primarily before 1920. Extreme heat days with a maximum temperature exceeding 40°C were rare. Before the 1940s, the occurrence of minimum temperatures above 25°C was considerably infrequent. But since the 1950s, the TN25 trend has significantly increased. The TN25c indices almost mirrored the fluctuations of the TN25 indices, whereas the rising trend of TN25Mc was slower, indicating shorter durations of extreme heat days for the 25°C threshold. Extreme heat days with minimum temperatures exceeding 28°C were largely exclusive to the past 30 yr and peaked in the 2000s. Extreme heat days with minimum temperatures surpassing 30°C were uncommon but occurred on several occasions during the latest 20 yr.

(4) Throughout the study period, there was no observable trend in the monthly temperature anomaly for Tmax, with only a slight increasing trend observed during the last 2 decades. On the other hand, the temperature anomaly variation of Tmin exhibited significant differences, with temperatures presenting negative anomalies prior to 1981 and positive anomalies thereafter, and showing noticeable warming trends each month. The anomaly values for Tave were negative before 1981 and then became positive, with an absolute value reduction compared to Tmin. TXx and TX90p did not exhibit any significant changes throughout the study period. Conversely, the anomaly changes for TNx and TN90p were more apparent, demonstrating a generally consistent upward trend of negative-then-positive characteristics in all months of the year. DTR presented distinct distributions of positive before and negative after values, where the period of positive–negative boundaries roughly fell into the 1970s. The monthly temperature anomalies reflected a significantly asymmetric change between Tmax and Tmin, indicating that Tmin underwent a more pronounced warming process than Tmax.

(5) The extreme temperatures and their associated indices exhibited a periodic trend in Wuhan. For the first half of the study period, most indices showed no significant changes and displayed a gently declining trend. However, during the latter half of the study period, the majority of indices showed an obvious uptick in temperature trends that passed the 0.05 significance level test. This trend may include significant urbanization effects over the last few decades in addition to background climate warming.

Acknowledgements. This study was financed by the National Key Research and Development Program of China (Fund No. 2018YFA0605603). We thank Dr. Panfeng Zhang, Dr. Kangmin Wen, Dr. Yun Qin, Dr. Xiaohui Ju, Dr. Xiaoying Xue, and Dr. Xiubao Sun for their contributions to the recovery and digitization of the early-period observation data for Wuhan.

LITERATURE CITED

Aguilar E, Auer I, Brunet M, Peterson TC, Wieringa J (2003) Guidelines on climate metadata and homogenization. WMO/TD No. 1186. World Meteorological Association, Geneva

Allan R, Brohan P, Compo GP, Stone R, Luterbacher J, Brönnimann S (2011) The international Atmospheric Circulation Reconstructions over the Earth (ACRE) initiative. Bull Am Meteorol Soc 92:1421–1425

Ansell TJ, Jones PD, Allan RJ, Lister D and others (2006) Daily mean sea level pressure reconstructions for the European-North Atlantic region for the period 1850–2003. J Clim 19: 2717–2742

Ashcroft L, Gergis J, Karoly DJ (2014) A historical climate dataset for southeastern Australia, 1788–1859. Geosci Data J 1:158–178

Camuffo D (2002) History of the long series of daily air temperature in Padova (1725–1998). Clim Change 53:7–75

Cao L, Zhu Y, Tang G, Yuan F, Yan Z (2016) Climatic warming in China according to a homogenized data set from 2419 stations. Int J Climatol 36:4384–4392

Chen ZH, Wang HJ, Ren G (2007) Asymmetrical change of urban heat island intensity in Wuhan, China. Adv Clim Chang Res 3:282–286

Cornes R (2008) The barometer measurements of the Royal Society of London: 1774–1842. Weather 63:230–235

Gui X, Wang L, Yao R, Yu D, Li C (2019) Investigating the urbanization process and its impact on vegetation change and urban heat island in Wuhan, China. Environ Sci Pollut Res Int 26:30808–30825

Handmer J, Honda Y, Kundzewicz ZW, Arnell N and others (2012) Changes in impacts of climate extremes: human systems and ecosystems. In: Field CB, Barros V, Stocker TF, Qin D and others (eds) Managing the risks of extreme events and disasters to advance climate change adaptation: A special report of Working Groups I and II of the Intergovernmental Panel on Climate Change. Cambridge University Press, Cambridge, p 231–290

He J, Ren G, Zhang P, Zheng X, Zhang S (2023) Updated analysis of surface warming trend in North China based on in-depth homogenized data (1951–2020). Clim Res 91:47–66

Hestmark G, Nordli O (2016) Jens Esmark's Christiania (Oslo) meteorological observations 1816–1838: the first long-term continuous temperature record from the Norwegian capital homogenized and analysed. Clim Past 12: 2087–2106

Hewaarachchi AP, Li Y, Lund R, Rennie J (2017) Homogenization of daily temperature data. J Clim 30:985–999

Hoerl AE, Kennard RW (1970) Ridge regression: biased estimation for nonorthogonal problems. Technometrics 12: 55–67

Hubei Meteorological Bureau (2018) Hubei Province Climate Change Bulletin. Wuhan. http://hb.cma.gov.cn/qxfw/qhyxpj/202012/t20201230_2548306.html (in Chinese)

Jia W, Ren G, Suo N, Zhang P, Wen K, Ren Y (2019) Urban heat island effect and its contribution to observed temperature increase at Wuhan station, Central China. J Trop Meteorol 25:102–113

Jones PD, Lister D, Osborn TJ, Harpham C, Salmon M, Morice C (2012) Hemispheric and large-scale land-surface air temperature variations: an extensive revision and an update to 2010. J Geophys Res 117:D05127

Lee TC, Chan HS, Ginn EWL, Wong MC (2011) Long-term trends in extreme temperatures in Hong Kong and southern China. Adv Atmos Sci 28:147–157

Lenssen NJL, Schmidt GA, Hansen J, Menne MJ, Persin A, Ruedy R, Zyss D (2019) 498 Improvements in the GISTEMP uncertainty model. J Geophys Res 124: 6307–6326

Liu Y, Ren G, Kang H, Sun X (2019) A significant bias of T_{max} and T_{min} average temperature and its trend. J Appl Meteorol Climatol 58:2235–2246

Luo M & Lau NC (2021) Increasing human-perceived heat stress risks exacerbated by urbanization in China: a comparative study based on multiple metrics. Earth's Future 9:e2020EF001848

Mann HB (1945) Nonparametric tests against trend. Econometrica 13:245–259

Menne MJ, Williams CN, Gleason BE, Rennie JJ, Lawrimore JH (2018) The global historical climatology network monthly temperature dataset, Version 4. J Clim 31: 9835–9854

Qin J, Zhang LJ, Hu JL (2000) Multi time scales analysis of climate variation in Wuhan during the last 100 years. Sci Meteorol Sin 21:206–210 (in Chinese)

Rasmussen R, Baker B, Kochendorfer J, Meyers T and others (2012) How well are we measuring snow: the NOAA/FAA/NCAR winter precipitation test bed. Bull Am Meteorol Soc 93:811–829

Ren GY, Zhou YQ (2014) Urbanization effects on trends of extreme temperature indices of national stations over mainland China, 1961–2008. J Clim 27:2340–2360

Ren GY, Chu ZY, Chen ZH, Ren YY (2007) Implications of temporal change in urban heat island intensity observed at Beijing and Wuhan stations. Geophys Res Lett 34: L05711

Ren YJ, Chen ZH, Xiao Y (2010) Surface air temperature change of last 100 years over Wuhan region. Dili Kexue 30:278–282 (in Chinese)

Ren GY, Li K, Ren YY, Chu ZY and others (2015) An integrated procedure to determine a reference station network for evaluating and adjusting urban bias in surface air temperature data. J Appl Meteorol Climatol 54: 1248–1266

Rohde R, Muller RA, Jacobsen R, Muller E and others (2013) A new estimate of the average earth surface land temperature spanning 1753 to 2011. Geoinfor Geostat An Overview 1:1

Rong G (2010) Trends of ten main extreme weather indices in Wuhan. Clim Chang Res 6:22–28 (in Chinese with English Abstract)

Sen PK (1968) Estimates of the regression coefficient based on Kendall's tau. J Am Stat Assoc 63:1379–1389

Shen SS, Somerville RC (2019) Climate mathematics. Cambridge University Press, Cambridge

Sun Y, Zhang XB, Ren GY, Zwiers FW, Hu T (2016) Contribution of urbanization to warming in China. Nat Clim Chang 6:706–709

Sun X, Wang C, Ren G (2021) Changes in the diurnal temperature range over East Asia from 1901 to 2018 and its relationship with precipitation. Clim Change 166:44

Tysa SK, Ren GY, Qin Y, Wen KM, Ren YY, Jia WQ, Zhang PF (2019) Urbanization effect in regional temperature series based on a remote-sensing classification scheme of stations. J Geophys Res Atmos 124:10646–10661

Vincent LA, Wang XL, Milewska EJ, Wan H, Yang F, Swail V (2012) A second generation of homogenized Canadian monthly surface air temperature for climate trend analysis. J Geophys Res D Atmospheres 117:D18110

Wang XL, Feng Y (2013) RHtestsV4 user manual. Climate Research Division, Atmospheric Science and Technology Directorate, Science and Technology Branch, Environment Canada, Toronto

Wang SW, Gong DY, Ye JL, Chen ZH (2000) Seasonal precipitation series of Eastern China since 1880 and the variability. Acta Geogr Sin 55:281–293 (in Chinese with English Abstract)

Xu XC, Ge QS, He SF, Zhang XZ, Xu XL, Liu GX (2016) Impact of high temperature on the mortality in summer of Wuhan, China. Environ Earth Sci 75:543

Xue X, Ren G, Sun X, Zhang P and others (2021) Change in mean and extreme temperature at Yingkou station in Northeast China from 1904 to 2017. Clim Change 164:58

Yan Z, Jones PD, Davies TD, Moberg A and others (2002) Trends of extreme temperatures in Europe and China based on daily observations. Clim Change 53:355–392

Yan JH, Liu HL, Ge QS, Zheng JY, Hao ZX, Wang YM (2017) Reconstruction and analysis of annual mean temperature of Wuhan for the 1906-2015 period. Prog Geogr 36:1176–1183 (in Chinese with English Abstract)

Yang YJ, Wu BW, Shi C, Zhang JH and others (2013) Impacts of urbanization and station-relocation on surface air temperature series in Anhui Province, China. Pure Appl Geophys 170:1969–1983

Yao WL, Chen ZH, Xiang YC (2010) Trends in climate extremes in association with climate warming in Wuhan. Qixiang 36:88–94 (in Chinese)

Yu J, Li QX, Zhang TW, Xu WH, Zhang L, Cui Y (2018) The merging test using measurements, paleoclimate reconstruction and climate model data based on Bayesian model. Acta Meteorol Sin 76:304–314 (in Chinese)

Yu X, Ren G, Zhang P, Hu J, Liu N, Li J, Zhang C (2020) Extreme temperature change of the last 110 years in Changchun, Northeast China. Adv Atmos Sci 37: 347–358

Zaiki M, Können GP, Tsukahara T, Jones PD, Mikami T, Matsumoto K (2006) Recovery of nineteenth-century Tokyo/Osaka meteorological data in Japan. Int J Climatol 26:399–423

Zhang X, Yang F (2004) RClimDex (1.0) user manual. Climate Research Branch, Environment Canada, Downsview, Ontario

Zhang X, Zwiers FW, Li G (2004) Monte Carlo experiments on the detection of trends in extreme values. J Clim 17: 1945–1952

Zhang L, Ren GY, Ren YY, Zhang AY, Chu ZY, Zhou YQ (2014) Effect of data homogenization on estimate of temperature trend: a case of Huairou station in Beijing Municipality. Theor Appl Climatol 115:365–373

Zhang Y, Feng R, Wu R, Zhong P, Tan X, Wu K, Ma L (2017) Global climate change: impact of heat waves under dif-

ferent definitions on daily mortality in Wuhan, China. Glob Health Res Policy 2:10

Zhang H, Luo M, Pei T, Liu XP and others (2023) Unequal urban heat burdens impede climate justice and equity goals. Innovation (Camb) 4:100488

Zheng ZF, Qi W, Zhang XL (2002) The character of temperature variation of Wuhan City during recent 95 years. Qixiang 28:18–21 (in Chinese)

Zheng JY, Liu Y, Ge QS, Hao ZX (2015) Spring phenodate records derived from historical documents and reconstruction on temperature change in Central China during 1850–2008. Acta Geogr Sin 70:696–704 (in Chinese)

Editorial responsibility: Eduardo Zorita, Geesthacht, Germany
Reviewed by: 3 anonymous referees

Submitted: May 28, 2023
Accepted: October 10, 2023
Proofs received from author(s): December 15, 2023